^{18}F-FDG Avidity of Pheochromocytomas and Paragangliomas: A New Molecular Imaging Signature?

David Taïeb[1], Frederic Sebag[2], Anne Barlier[3], Laurent Tessonnier[1], Fausto F. Palazzo[2], Isabelle Morange[4], Patricia Niccoli-Sire[4], Nicolas Fakhry[5], Catherine De Micco[6], Serge Cammilleri[1], Alain Enjalbert[3], Jean-François Henry[2], and Olivier Mundler[1]

[1]Service Central de Biophysique et de Médecine Nucléaire, Centre Hospitalo-Universitaire de la Timone, Marseille, France; [2]Service de Chirurgie Générale et Endocrinienne, Centre Hospitalo-Universitaire de la Timone, Marseille, France; [3]Laboratoire de Biochimie et Biologie Moléculaire, Centre Hospitalier Universitaire Conception, Marseille, France; [4]Service d'Endocrinologie, Diabète et Métabolismes, Centre Hospitalo-Universitaire de la Timone, Marseille, France; [5]Service D'oto-Rhino-Laryngologie, Centre Hospitalo-Universitaire de la Timone, Marseille, France; and [6]Faculté de Médecine, Institut National de la Santé et de la Recherche Médicale, Marseille, France

Our objective was to evaluate ^{18}F-FDG PET uptake in patients with nonmetastatic and metastatic chromaffin-derived tumors. **Methods:** Twenty-eight consecutive unrelated patients with chromaffin tumors, including 9 patients with genetically determined disease, were studied. A combination of preoperative imaging work-up, surgical findings, and pathologic analyses was used to classify the patients into 2 groups: those with nonmetastatic disease (presumed benign, $n = 18$) and those with metastatic tumors ($n = 10$). ^{18}F-FDG PET was performed in all cases. Visual and quantitative analyses were individually graded for each tumor. Somatic mutations of the succinate dehydrogenase subunits B and D and Von-Hippel Lindau genes were also evaluated in 6 benign sporadic tumor samples. **Results:** All but 2 patients showed significantly increased ^{18}F-FDG uptake on visual analysis. The maximum standardized uptake value (SUVmax) ranged from 1.9 to 42 (mean ± SD, 8.2 ± 9.7; median, 4.6) in nonmetastatic tumors and 2.3 to 29.3 (mean ± SD, 9.7 ± 8.4; median, 7.4) in metastatic tumors. No statistical difference was observed between the groups ($P = 0.44$), but succinate dehydrogenase–related tumors were notable in being the most ^{18}F-FDG–avid tumors (SUVmax, 42, 29.3, 21, 17, and 5.3). Succinate dehydrogenase and Von-Hippel Lindau–related tumors had a significantly higher SUVmax than did neurofibromatosis type 1 and multiple endocrine neoplasia type 2A syndrome–related tumors ($P = 0.02$). ^{18}F-FDG PET was superior to ^{131}I-metaiodobenzylguanidine in all metastatic patients but one. By contrast, ^{18}F-FDG PET underestimated the extent of the disease, compared with 6-^{18}F-fluorodopa PET, in 5 patients with metastatic pheochromocytoma. However, succinate dehydrogenase mutations (germline and somatic) and functional dedifferentiation do not adequately explain ^{18}F-FDG uptake since most tumors were highly avid for ^{18}F-FDG. **Conclusion:** ^{18}F-FDG PET positivity is almost a constant feature of pheochromocytomas and paragangliomas. It may be considered a molecular signature of such tumors, although which aspect of the plethora of molecular changes associated with dedifferentiation, germline genetic defects, or the adaptive response to hypoxia is responsible for this characteristic requires further elucidation.

Key Words: molecular imaging; PET/CT; neuroendocrine; FDG PET; pheochromocytoma; Warburg effect

J Nucl Med 2009; 50:711–717
DOI: 10.2967/jnumed.108.060731

Pheochromocytomas and extraadrenal paragangliomas are rare tumors of neuroectodermal origin. They belong to the heterogeneous family of neuroendocrine tumors and present a spectrum of SPECT- and PET-targetable distinctive phenotypic markers such as amine precursor uptake and decarboxylation and the overexpression of peptide receptors. Previously, ^{18}F-FDG PET has not been widely used in oncoendocrinology because of a lack of specificity (*1*). However, the mechanisms that control glucose uptake are numerous and potentially include molecular changes involved in neuroendocrine tumors (*2*).

Endocrine tumors (i.e., follicle-derived thyroid carcinoma, medullary thyroid carcinomas, and pancreatic tumors) generally exhibit a 2-phase metabolic profile with an initially low or absent ^{18}F-FDG uptake followed by an increased ^{18}F-FDG uptake in the later stages of the disease (*3–5*). Chromaffin-derived tumors do not appear to follow this pattern of tracer uptake of other endocrine tumors.

^{18}F-FDG PET has proved to be an effective tool in the localization of metastatic succinate dehydrogenase subunit B (SDHB) paraganglioma (*6,7*), and our group has reported that, compared with other imaging modalities alone, ^{18}F-FDG provides additional information in patients with metastatic and multifocal forms of pheochromocytoma (*8*).

Received Nov. 30, 2008; revision accepted Feb. 3, 2009.
For correspondence or reprints contact: David Taïeb, Service Central de Biophysique et de Médecine Nucléaire, Centre Hospitalo-Universitaire de la Timone, 264 Rue Saint-Pierre 13385 Marseille Cedex 5, France.
E-mail: david.taieb@ap-hm.fr

However, enhanced ^{18}F-FDG uptake has also been reported in benign pheochromocytomas, without any correlation with catecholamine levels (*9,10*).

Despite the growing clinical relevance of ^{18}F-FDG PET, little is known about the molecular determinants of tracer uptake in different types of tumors. Enhanced uptake and metabolism of glucose, a frequent characteristic of most cancer cells, is associated with an alteration in the intrinsic energy metabolism causing a shift from oxidative phosphorylation to aerobic glycolysis, a change referred to as the Warburg effect (*11*). Because glycolysis is considerably less efficient than oxidative phosphorylation at producing adenosine triphosphate, the tumor cell requires an acceleration in the rate of glucose uptake and use. The molecular mechanisms that underpin metabolic reprogramming of cancer cells are complex and involve adaptive responses to the tumor microenvironment, such as hypoxia, or mutations in enzymes or oncogenes that control cell metabolism (*12*). Several studies have demonstrated that ^{18}F-FDG uptake is an indirect reflection of tumor hypoxia (*13*).

The aim of this study was to ascertain whether ^{18}F-FDG uptake is associated with malignancy or is related to a specific metabolic pattern associated with these tumors irrespective of their clinical behavior.

MATERIALS AND METHODS

Patients

Twenty-eight unrelated patients (20 men, 8 women; age range, 25–78 y) with pheochromocytomas or paragangliomas, including 12 cases of persistent or recurrent disease and 16 cases of newly diagnosed disease, were included in this retrospective study.

Four patients had a family history of pheochromocytoma or paraganglioma, and in 5 additional patients genetic testing identified predisposing mutations. Four of the patients had SDHB, 1 had succinate dehydrogenase subunit D (SDHD), 1 had multiple endocrine neoplasia type 2A (MEN-2A), 2 had neurofibromatosis type 1 (NF1), and 1 had Von-Hippel Lindau (VHL). As the definition of malignancy may appear ambiguous in paraganglioma since a primary nonmetastatic tumor may later develop into metastases, the term *malignant* was avoided and *metastatic* preferred (*14*). Using results from preoperative imaging work-up, we classified patients into 2 groups based on final disease status: nonmetastatic tumors (n = 18) and metastatic tumors (n = 10). The first group included 8 patients with unifocal sporadic disease and 10 with multicentric or genetically predisposed disease. Imaging work-up comprised at least full-body CT and molecular imaging studies including ^{131}I-metaiodobenzylguanidine scintigraphy (in 25 patients), ^{111}In-octreotide scintigraphy (somatostatin receptor scintigraphy) (in 6 patients), 6-^{18}F-fluorodopa PET (in 19 patients), and ^{99m}Tc-hydroxymethylenediphosphonate bone scintigraphy (in 5 patients) (Table 1).

The patient characteristics are summarized in Table 1. Data from 8 of these patients have been previously reported in a preliminary study (*8*).

In patients with unifocal disease, the tumor diameters ranged from 12 to 58 mm (median, 34 mm). In patient 15, one of the pheochromocytomas was associated with hemorrhagic necrosis.

Genetic Testing

SDHB, SDHD, and VHL genes were amplified using exon flanking from DNA isolated from the blood samples of all patients bearing pheochromocytomas or paragangliomas in the absence of other lesions suggestive of MEN-2A or NF1 syndrome. The same primers were used for sequencing using a CEQ 8000 sequencer (Beckman Coulter) and are available on request. SDHB and SDHD gene analysis was also performed on 6 frozen tissue samples (T1, T2, T4–T6, and T8) taken from sporadic tumors (without germinal mutation).

^{18}F-FDG PET Scanning

Patients fasted for a minimum of 6 h before the tracer injection (4 MBq/kg), and scanning began 60 min later. Three-dimensional images were acquired from the skull base to the upper thigh using a Discovery ST PET/CT scanner (GE Healthcare). CT was performed first, from the head to the upper thigh, with 140 kV, 80 mA, and a 5-mm section thickness, which matched the PET section thickness. Immediately after the CT scan, a PET scan was obtained that covered the identical transverse field of view with an acquisition time of 3 min per table position. PET image datasets were reconstructed iteratively (ordered-subsets expectation maximization algorithm) using CT data for attenuation correction. Coregistered images were displayed on a workstation (Xeleris; GE Healthcare), with 3-dimensional representation as well as axial, coronal, and sagittal slices.

Image Interpretation and Quantitative Measurements

All ^{18}F-FDG PET/CT scans were interpreted independently by 2 experienced nuclear medicine physicians. The physicians were unaware of the findings of other imaging studies, including nuclear and conventional morphologic imaging. Visual and quantitative analyses were individually graded for each tumor. In pheochromocytomas, ^{18}F-FDG uptake was compared qualitatively between the tumor and the liver. The PET/CT finding was considered positive if ^{18}F-FDG uptake looked markedly higher in the adrenal tumor than in the liver and negative if ^{18}F-FDG uptake in the adrenal tumor looked less than, the same as, or slightly higher than that in the liver. In paragangliomas, the ^{18}F-FDG PET finding was considered positive if ^{18}F-FDG uptake was markedly higher in the tumor than in the surrounding normal tissue.

A region of interest was drawn on the tumor. Activity counts in the regions of interest were normalized to injected doses per kilogram of patient body weight (maximum standardized uptake value [SUVmax]). We then measured SUVmax in the region of interest on the PET images.

Statistical Analysis

SUVmax (assessed from the most avid focus, one per patient) was compared between tumor groups using the Wilcoxon signed-rank test (SPSS software, version 15.0 [SPSS Inc.], for Windows). A P value of less than 0.05 was considered statistically significant.

RESULTS

Nonmetastatic Tumors

All but 2 tumors had an increased ^{18}F-FDG uptake on visual analysis. SUVmax ranged from 1.9 to 42 (mean ± SD, 8.1 ± 9.7; median, 4.6).

TABLE 1. Patient and Tumor Characteristics

Patient no.	Initial presentation	Indication	Sex	Age (y)	Final status	^{18}F-FDG PET foci	VA	SUVmax	Molecular imaging technique	Additional foci on ^{18}F-FDG PET, compared with...*		Germline mutation
										SPECT	FDOPA	
1	Pheo	Initial staging	F	58	Unifocal	Adrenal	Pos	3.5	MIBG	No (=)	ND	Absent
2	Pheo	Initial staging	F	30	Unifocal	Adrenal	Pos	12	MIBG	No (=)	ND	Absent
3	Pheo	Initial staging	M	38	Unifocal	Adrenal	Pos	11	FDOPA	ND	No (=)	Absent
4	Pheo	Initial staging	M	30	Unifocal	Adrenal	Neg	2.1	MIBG, FDOPA	No (=)	No (<)	Absent
5	Pheo	Initial staging	F	26	Unifocal	Adrenal	Pos	9.5	MIBG	No (=)	ND	Absent
6	Ab PGL	Initial staging	M	64	Unifocal	Ab PGL	Pos	4.5	MIBG	No (=)	ND	Absent
7	Ab PGL	Initial staging	F	52	Unifocal	Ab PGL	Pos	5.7	MIBG, FDOPA, SRS	No (=)	No (=)	Absent
8	Pheo	Initial staging	F	30	Unifocal	Adrenal	Pos	3.8	FDOPA	—	ND	Absent
9	Pheo	Initial staging	M	34	Unifocal	Adrenal	Pos	42	MIBG	No (=)	ND	SDHB
10	Pheo	Recurrence	M	25	Multifocal	Adrenal, ab PGL (renal pedicle)	Pos	6	MIBG, FDOPA, SRS	Yes	No (=)	VHL
11	Pheo + PGL	Initial staging	M	34	Multifocal	Ab and ce PGL (gl)	Pos	21	MIBG, FDOPA, SRS	Yes	Yes	SDHD
12	Ce PGL	Initial staging	M	67	Multifocal	Ce PGL (gl + vagal)	Pos	3.5	SRS, FDOPA	No (=)	No (=)	Absent
13	Pheo	Recurrence	M	70	Multifocal	Ce PGL (gl)	Pos	5.3	MIBG, FDOPA, SRS	No (=)	No (=)	SDHB
14	Pheo + PGL	Recurrence	M	56	Multifocal	Ab PGL	Pos	3.9	MIBG	Yes	ND	ND
15	Pheo	Initial staging	M	36	Multifocal	Adrenal (bilateral)	Pos	3.7	MIBG	No (=)	ND	Absent
16	Pheo	Initial staging	M	51	Unifocal	Adrenal	Pos	4.7	MIBG	No (=)	ND	NF1
17	Pheo	Initial staging	M	45	Unifocal	Adrenal	Neg	1.9	MIBG, FDOPA	No (=)	No (<)	NF1
18	Pheo	Recurrence	M	35	Multifocal	Adrenal	Pos	2	MIBG	No (=)	ND	RET
19	Pheo	Recurrence	F	61	Metastatic	Lung, me, carcinosis	Pos	4.5	MIBG, FDOPA	Yes	No (=)	Absent
20	Pheo	Recurrence	M	75	Metastatic	Adrenal, Lung, me, liver, LN	Pos	13.3	MIBG, FDOPA	Yes	Yes	Absent
21	Pheo	Recurrence	F	32	Metastatic	Lung, liver, bone	Pos	2.3	MIBG, FDOPA	Yes	No (<)	Absent
22	Pheo	Recurrence	M	34	Metastatic	Liver, bone	Pos	9.9	MIBG, FDOPA, HMDP	No (<)	No (<)	Absent
23	Pheo	Recurrence	M	43	Metastatic	Lung, liver, LN	Pos	3.3	MIBG, FDOPA, HMDP	Yes	No (<)	Absent
24	PGL	Recurrence	M	78	Metastatic	Ab PGL, bone	Pos	7	MIBG, FDOPA, HMDP	Yes	Yes	Absent
25	PGL	Recurrence	F	59	Metastatic	Lung, LN, Bone	Pos	3	MIBG, FDOPA, HMDP, SRS	Yes	No (<)	Absent
26	Pheo	Initial staging	M	63	Metastatic	Adrenal, Bone	Pos	7.8	MIBG, FDOPA	Yes	No (<)	ND
27	PGL	Recurrence	M	38	Metastatic	Ab and ce PGL, LN	Pos	29.3	MIBG, FDOPA	Yes	Yes	SDHB
28	Pheo	Initial staging	M	34	Metastatic	Adrenal, Bone	Pos	17	MIBG, HMDP	Yes	ND	SDHB

VA = visual analysis; FDOPA = 6-^{18}F-fluorodopa PET; pheo = pheochromocytoma; pos = positive; MIBG = ^{131}I-MIBG; ND = not done; ab = abdominal; PGL = paraganglioma; SRS = somatostatin receptor scintigraphy; ce = cervical; gl = glomic; neg = negative; RET = RET protooncogene; me = mediastinal; LN = lymph node; HMDP = ^{99m}Tc-HMDP; HMDP = hydroxymethylenediphosphonate.

*Comparison between ^{18}F-FDG PET and SPECT (^{131}I-metaiodobenzylguanidine [MIBG] or SRS) and 6-^{18}F-fluorodopa PET studies in terms of number of tumor sites. = indicates equivalent number of tumor sites on ^{18}F-FDG PET; < indicates lower number of tumor sites on ^{18}F-FDG PET; > indicates higher number of tumor sites on ^{18}F-FDG PET.

The first false-negative result corresponded to a pheochromocytoma with a 12-mm diameter and a SUVmax ratio (tumor to liver) of 1.2 (patient 4). The second false-negative result (SUVmax of 1.9 and ratio of 1.3) corresponded to a 15-mm-diameter NF1-associated mixed neoplasm composed of a combined pheochromocytoma and ganglioneuroma (patient 17). Interestingly, both tumors had negative ^{131}I-metaiodobenzylguanidine findings but were positive on 6-^{18}F-fluorodopa PET. The other tumors had positive ^{18}F-FDG PET findings, including a 10-mm MEN-

2A–related pheochromocytoma (patient 18). In patient 12, despite the large volume of the glomic paraganglioma and in comparison with a unifocal pheochromocytoma, SUVmax was lower than expected. In patient 11 (SDHD-positive), the SUVmax was higher in the abdominal foci than in the neck, 21 versus 8.1, respectively. Compared with ^{131}I-metaiodobenzylguanidine scanning and 6-^{18}F-fluorodopa PET, ^{18}F-FDG PET identified additional lesions in 3 and 1 patients, respectively, with multifocal disease.

Some examples are illustrated in Figure 1.

Metastatic Tumors

All patients had positive ^{18}F-FDG PET findings. The SUVmax ranged from 2.3 to 29.3 (mean ± SD, 9.7 ± 8.4; median, 7.4) (Figs. 1 and 2). Compared with ^{131}I-metaiodobenzylguanidine scanning, ^{18}F-FDG PET identified additional tumor sites in all patients but one. By contrast, ^{18}F-FDG PET underestimated the extent of the disease, compared with 6-^{18}F-fluorodopa PET, in 5 patients with metastatic pheochromocytoma (patients 21, 22, 23, 25, and 26) (Fig. 3). These tumors corresponded to the most differentiated lesions on the basis on the molecular imaging procedures performed.

Comparison of ^{18}F-FDG Uptake Between Tumors

All but 2 patients had significantly increased ^{18}F-FDG uptake on visual analysis without a statistical difference in SUVmax between nonmetastatic tumors (presumed benign) and metastatic tumors (P = 0.44) (Fig. 4). Interestingly, SDH-related tumors were notable in being the most ^{18}F-FDG–avid tumors (SUVmax, 42, 29.3, 21, 17, and 5.3). SDH- and VHL-related tumors had a significantly higher SUVmax than did tumors related to NF1 and MEN-2A syndromes (P = 0.02).

Somatic Mutation Analyses

No somatic mutations of the SDHB, SDHD, or VHL genes were detected in tissue samples.

DISCUSSION

Our series of 28 patients had just 2 tumors without significant ^{18}F-FDG uptake on visual analysis. In keeping with previous reports, we confirm that ^{18}F-FDG PET adds value to other molecular imaging techniques in some cases of multifocal or metastatic disease (*6–8*). We strongly recommend that ^{18}F-FDG PET be performed in cases of metastatic or non–SDH-related tumors.

It is noteworthy that, even in benign tumors, SUVmax was as high as is usually observed in primary or secondary malignant adrenal tumors (*15*). We are unaware of any other benign tumor with such high levels of glucose uptake. In one of the negative (on visual imaging) ^{18}F-FDG PET patients, the tumor demonstrated nonclassic clinicopathologic features, with a mixed pheochromocytoma and ganglioneuroma neoplasm in the context of an NF1-related tumor.

Paragangliomas, because they derive from neuroectodermal cells, would be expected to share a functional glucose-metabolic pattern in common with active neurons. However, in contrast to normal cerebral cortex, normal adrenal glands are rarely visualized by PET despite the 4- to 6-mm spatial resolution achieved with the bismuth germanate–based GE Discovery ST PET/CT scanner.

Although we concur with the view of Timmers et al. (*6*) that in cases of metastatic disease ^{18}F-FDG PET should be

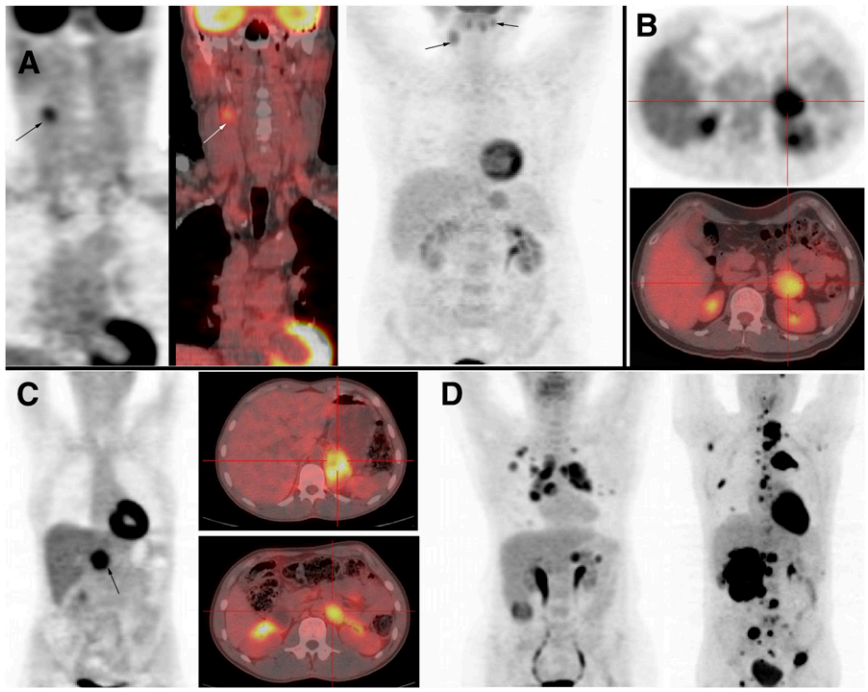

FIGURE 1. (A) Cervical paraganglioma (patients 13 and 12): Patient 13 is SDHB patient with right glomic paraganglioma (arrow), as seen on coronal ^{18}F-FDG PET (left) and fusion imaging (middle). Patient 12 has bilateral cervical paraganglioma, as seen on coronal ^{18}F-FDG PET (right). (B) Left pheochromocytoma (patient 3), as seen on axial ^{18}F-FDG PET (top) and fusion imaging (bottom). (C) Abdominal nonmetastatic tumors (patients 7 and 10): Patient 7 has abdominal right paraganglioma, as seen on coronal ^{18}F-FDG PET (left). Patient 10 is VHL patient with left pheochromocytoma (top right) and paraganglioma at left renal hilum (bottom right), as seen on axial fusion imaging. (D) Metastatic pheochromocytoma (patients 19 and 28): Patient 19 has recurrent pheochromocytoma, as seen on maximum-intensity-projection image (left). Patient 28 is SDHB patient with metastatic pheochromocytoma, as seen on maximum-intensity-projection image (right).

RGB

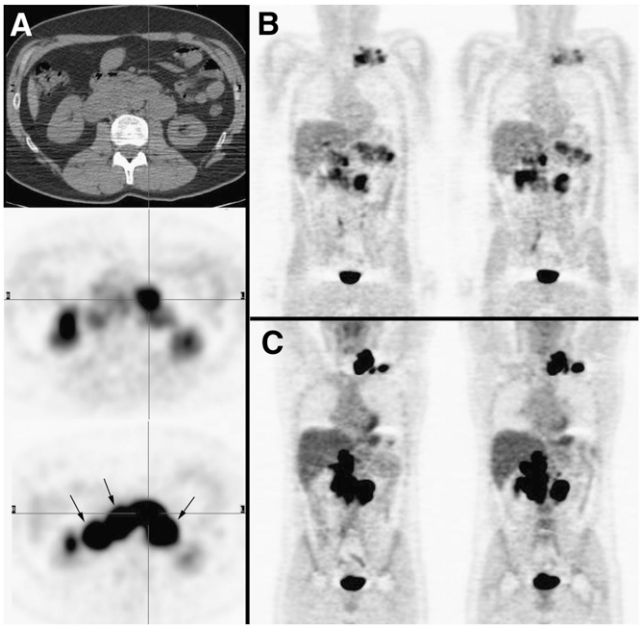

FIGURE 2. Metastatic SDHB-related pheochromocytoma (patient 27): multiple abdominal paraganglioma seen on axial CT (top), axial 6-^{18}F-fluorodopa PET (middle), and axial ^{18}F-FDG PET (bottom) (A); 6-^{18}F-fluorodopa PET (coronal whole-body axial images) (B); and ^{18}F-FDG PET (coronal whole-body axial images) (C). Compared with 6-^{18}F-fluorodopa PET, ^{18}F-FDG PET detected additional tumor sites and ^{18}F-FDG PET avidity was higher (arrow).

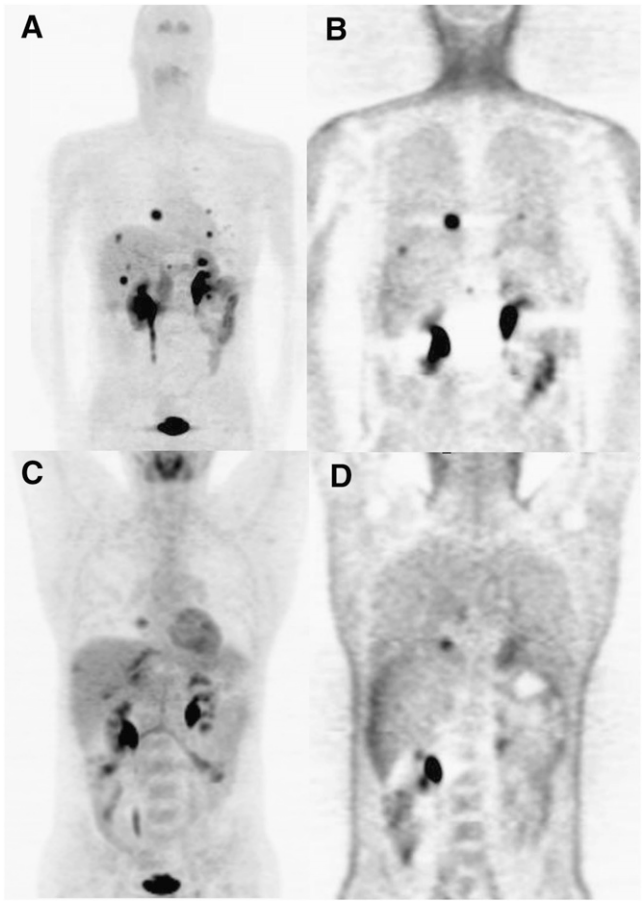

FIGURE 3. Metastatic sporadic pheochromocytoma (patient 23): 6-^{18}F-fluorodopa PET maximum-intensity-projection image (A), ^{18}F-FDG PET maximum-intensity-projection image (B), attenuation-uncorrected 6-^{18}F-fluorodopa PET coronal image (C), and attenuation-uncorrected ^{18}F-FDG PET coronal image (D). Compared with 6-^{18}F-fluorodopa PET, ^{18}F-FDG PET underestimated extent of disease.

considered a marker of functional dedifferentiation, functional dedifferentiation alone does not explain ^{18}F-FDG uptake in all cases because benign pheochromocytomas are highly ^{18}F-FDG–avid. Indeed, the series of Timmers et al. included SDHB-related tumors, in which such mutations can participate in the metabolic reprogramming that is known to occur in tumor cells.

Our findings and data from the related literature may support 2 additional alternative explanations: that an early metabolic switch related to genetic defects occurs (pseudohypoxia model) or that an adaptive response to hypoxia occurs. These possibilities would explain why the ^{18}F-FDG avidity of pheochromocytomas and paragangliomas seems to be different from that of other neuroendocrine tumors, in which ^{18}F-FDG uptake tends to be related to dedifferentiation and aggressiveness, such as in thyroid cancers and endocrine pancreatic tumors.

We hypothesize that the amount of glucose uptake in chromaffin-derived tumors results from the severe impairment of oxidative phosphorylation in tumor cells. One theory that links pheochromocytomas and increased ^{18}F-FDG uptake is based on a pseudohypoxia model. In support of this theory is the fact that these tumors are also highly vascularized—a hallmark of a hypoxic response. Some pheochromocytomas are caused by a germline mutation in VHL or SDH tumor suppressor genes (SDHB, SDHC, and SDHD) (*16*). The pseudohypoxia model implies a link between inactivation of SDH and VHL and induction of a hypoxic response under normal oxygen conditions (*17*), a response mediated by the oxygen-regulated transcription factor hypoxia-inducible factor 1α. Under normal oxygen conditions, hypoxia-inducible factor 1α is rapidly degraded by the ubiquitin-proteasome system, which is mediated by the VHL-E3 ubiquitin ligase pathway. In addition, VHL recognizes hypoxia-inducible factor 1α only after prolyl hydroxylations by a family of dioxygenases, termed prolyl hydroxylase domain proteins, that use oxygen as a cosubstrate. Thus, VHL inactivation or prolyl hydroxylase domain protein inhibition could lead to the stabilization of hypoxia-inducible factor 1α, which in turn activates target glycolytic enzyme genes and inhibits the tricarboxylic acid cycle. SDH mutations have been reported to inhibit prolyl hydroxylase domain proteins via an overproduction of reactive oxygen species and an accumulation of succinate

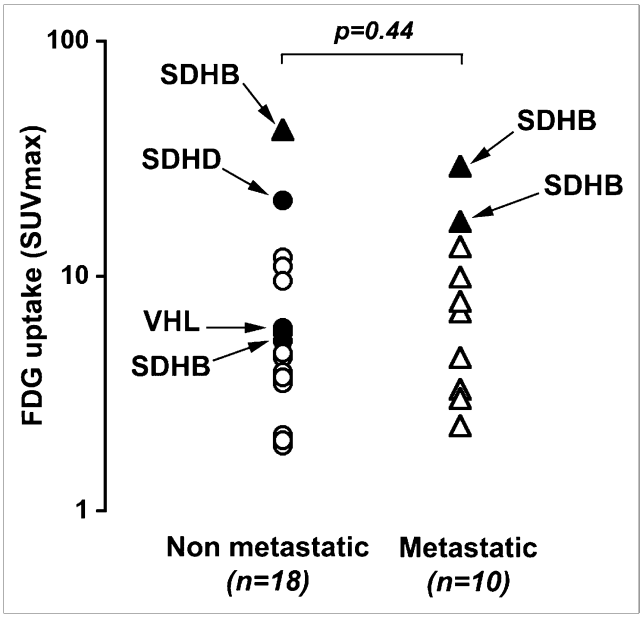

FIGURE 4. Comparison of SUVmax between nonmetastatic and metastatic tumors. Distributed values of SUVmax are represented. Mean SUVmax was not significantly different between tumors ($P = 0.44$). SDHB-related tumors were notable in being most ^{18}F-FDG–avid tumors (SUVmax, 42, 29.3, 21, and 17).

(*18,19*). This report would explain what occurs in tumors that carry mutations in VHL or SDH genes. New genetic defects involved in paraganglioma that potentially modulate tumor metabolism need to be identified (*20–22*).

However, genetically predisposed pheochromocytomas do not occur in all patients, and somatic mutations are uncommon in such tumors (*23,24*). In our series, no somatic mutation was found in unifocal, sporadic disease. Furthermore, all but one patient without any germinal mutation had increased ^{18}F-FDG, and glucose avidity was as intense in benign pheochromocytomas as in multifocal benign disease, which is at a higher risk of being associated with predisposing genetic events. However, there remain familial clusters of pheochromocytomas for which the primary genetic mutation has not yet been identified, the implication being that unknown potential genes involved in glucose metabolism could have been mutated in our patients (*25,26*). Furthermore, posttranslational protein modifications such as impairment in alternative splicing or variation in protein expression or activities are also possible and require evaluation in further basic science research (*27*).

Another hypothesis to explain such an SUVmax in pheochromocytomas is that a high rate of glycolysis is advantageous to tumor growth in this particular microenvironment. It has been well described that, as in our patient 15, pheochromocytomas can be associated with hemorrhagic remodeling caused by ischemia. The preferential use of glycolysis by tumor cells may provide cells with a competitive advantage under conditions of hypoxia (*28*). Even if ^{18}F-FDG does not correlate with secretory status, it is remarkable that some pheochromocytomas exhibit such a high SUVmax. We also know that catecholamine tonus fluctuates both quantitatively and qualitatively in pheochromocytomas. Thus, pheochromocytomas can survive and thrive in conditions of fluctuating oxygen tension resulting from unstable blood vessel hemodynamics that would be lethal for tumor cells relying on oxidative phosphorylation alone to generate adenosine triphosphate (*2*).

CONCLUSION

The present study highlights the relationship between genotype-specific metabolite analysis in paraganglioma and functional imaging characteristics. We found that ^{18}F-FDG uptake is remarkably common in pheochromocytomas and paragangliomas and should be considered a new molecular imaging hallmark. The metabolic pattern is probably complex and most likely involves dedifferentiation (in metastatic patients), specific genetic defects (in inherited forms), and adaptive responses to hypoxia (in sporadic pheochromocytomas). Further basic science studies and imaging research using tumor hypoxia imaging tracers are needed before conclusions can be drawn about the exact mechanisms responsible.

REFERENCES

1. Eriksson B, Orlefors H, Oberg K, Sundin A, Bergstrom M, Langstrom B. Developments in PET for the detection of endocrine tumours. *Best Pract Res Clin Endocrinol Metab.* 2005;19:311–324.
2. Pouyssegur J, Dayan F, Mazure NM. Hypoxia signalling in cancer and approaches to enforce tumour regression. *Nature.* 2006;441:437–443.
3. Adams S, Baum R, Rink T, Schumm-Drager PM, Usadel KH, Hor G. Limited value of fluorine-18 fluorodeoxyglucose positron emission tomography for the imaging of neuroendocrine tumours. *Eur J Nucl Med.* 1998;25:79–83.
4. Koopmans KP, de Groot JW, Plukker JT, et al. ^{18}F-dihydroxyphenylalanine PET in patients with biochemical evidence of medullary thyroid cancer: relation to tumor differentiation. *J Nucl Med.* 2008;49:524–531.
5. Robbins RJ, Wan Q, Grewal RK, et al. Real-time prognosis for metastatic thyroid carcinoma based on 2-[^{18}F]fluoro-2-deoxy-D-glucose-positron emission tomography scanning. *J Clin Endocrinol Metab.* 2006;91:498–505.
6. Timmers HJ, Kozupa A, Chen CC, et al. Superiority of fluorodeoxyglucose positron emission tomography to other functional imaging techniques in the evaluation of metastatic SDHB-associated pheochromocytoma and paraganglioma. *J Clin Oncol.* 2007;25:2262–2269.
7. Zelinka T, Timmers HJ, Kozupa A, et al. Role of positron emission tomography and bone scintigraphy in the evaluation of bone involvement in metastatic pheochromocytoma and paraganglioma: specific implications for succinate dehydrogenase enzyme subunit B gene mutations. *Endocr Relat Cancer.* 2008; 15:311–323.
8. Taieb D, Tessonnier L, Sebag F, et al. The role of ^{18}F-FDOPA and ^{18}F-FDG-PET in the management of malignant and multifocal phaeochromocytomas. *Clin Endocrinol (Oxf).* 2008;69:580–586.
9. Pauwels EK, Sturm EJ, Bombardieri E, Cleton FJ, Stokkel MP. Positron-emission tomography with [^{18}F]fluorodeoxyglucose. Part I. Biochemical uptake mechanism and its implication for clinical studies. *J Cancer Res Clin Oncol.* 2000;126:549–559.
10. Shulkin BL, Koeppe RA, Francis IR, Deeb GM, Lloyd RV, Thompson NW. Pheochromocytomas that do not accumulate metaiodobenzylguanidine: localization with PET and administration of FDG. *Radiology.* 1993;186:711–715.
11. Warburg O. *The Metabolism of Tumors.* London, U.K.: Arnold Constable; 1930.
12. Kroemer G, Pouyssegur J. Tumor cell metabolism: cancer's Achilles' heel. *Cancer Cell.* 2008;13:472–482.
13. Dierckx RA, Van de Wiele C. FDG uptake, a surrogate of tumour hypoxia? *Eur J Nucl Med Mol Imaging.* 2008;35:1544–1549.

14. Tischler AS. Pheochromocytoma: time to stamp out "malignancy"? *Endocr Pathol.* 2008;19:207–208.
15. Tessonnier L, Sebag F, Palazzo FF, et al. Does ^{18}F-FDG PET/CT add diagnostic accuracy in incidentally identified non-secreting adrenal tumours? *Eur J Nucl Med Mol Imaging.* 2008;35:2018–2025.
16. Neumann HP, Bausch B, McWhinney SR, et al. Germ-line mutations in nonsyndromic pheochromocytoma. *N Engl J Med.* 2002;346:1459–1466.
17. Gottlieb E, Tomlinson IP. Mitochondrial tumour suppressors: a genetic and biochemical update. *Nat Rev Cancer.* 2005;5:857–866.
18. Pollard PJ, Briere JJ, Alam NA, et al. Accumulation of Krebs cycle intermediates and over-expression of HIF1alpha in tumours which result from germline FH and SDH mutations. *Hum Mol Genet.* 2005;14:2231–2239.
19. Selak MA, Armour SM, MacKenzie ED, et al. Succinate links TCA cycle dysfunction to oncogenesis by inhibiting HIF-alpha prolyl hydroxylase. *Cancer Cell.* 2005;7:77–85.
20. Lee S, Nakamura E, Yang H, et al. Neuronal apoptosis linked to EglN3 prolyl hydroxylase and familial pheochromocytoma genes: developmental culling and cancer. *Cancer Cell.* 2005;8:155–167.
21. Schlisio S, Kenchappa RS, Vredeveld LC, et al. The kinesin KIF1Bbeta acts downstream from EglN3 to induce apoptosis and is a potential 1p36 tumor suppressor. *Genes Dev.* 2008;22:884–893.
22. Yeh IT, Lenci RE, Qin Y, et al. A germline mutation of the KIF1B beta gene on 1p36 in a family with neural and nonneural tumors. *Hum Genet.* 2008;124: 279–285.
23. Korpershoek E, Petri BJ, van Nederveen FH, et al. Candidate gene mutation analysis in bilateral adrenal pheochromocytoma and sympathetic paraganglioma. *Endocr Relat Cancer.* 2007;14:453–462.
24. van Nederveen FH, Korpershoek E, Lenders JW, de Krijger RR, Dinjens WN. Somatic SDHB mutation in an extraadrenal pheochromocytoma. *N Engl J Med.* 2007;357:306–308.
25. Astuti D, Hart-Holden N, Latif F, et al. Genetic analysis of mitochondrial complex II subunits SDHD, SDHB and SDHC in paraganglioma and phaeochromocytoma susceptibility. *Clin Endocrinol (Oxf).* 2003;59:728–733.
26. Dahia PL, Hao K, Rogus J, et al. Novel pheochromocytoma susceptibility loci identified by integrative genomics. *Cancer Res.* 2005;65:9651–9658.
27. Christofk HR, Vander Heiden MG, Harris MH, et al. The M2 splice isoform of pyruvate kinase is important for cancer metabolism and tumour growth. *Nature.* 2008;452:230–233.
28. Gatenby RA, Gillies RJ. Why do cancers have high aerobic glycolysis? *Nat Rev Cancer.* 2004;4:891–899.